

INFLUENCE OF THE IMPELLER TYPE ON DROP SIZE IN LIQUID-LIQUID DISPERSIONS

W. Podgórska

*Faculty of Chemical and Process Engineering, Warsaw University of Technology, ul.
Waryńskiego 1, 00645 Warsaw, Poland; e-mail: podgorsw@ichip.pw.edu.pl*

Abstract. The influence of impeller type on DSD is considered in this paper. Effects of application of two impellers including high power number, high shear impeller (6 blade Rushton turbine, RT) and 3 blade low power number, high efficiency impeller (HE3). Flow field and properties of turbulence in the agitated vessel (energy dissipation rate and scale of large eddies) are determined using the k- ϵ model of turbulence. Intermittency of turbulence is taken into account in breakage and coalescence models by using multifractal formalism. The solution of population balance equation for lean dispersions (pure breakage) with dispersed phase of low as well as high viscosity have shown that at equal power input per unit mass HE3 impeller produces much smaller droplets. In the case of fast coalescence (low dispersed phase viscosity) the model predicts similar droplets generated by both impellers. In the case of dispersed phase of high viscosity HE3 produces slightly smaller droplets.

Key words: Breakage; Coalescence; High efficiency impeller; Intermittency; Rushton turbine

1. INTRODUCTION

The liquid-liquid dispersions in turbulent flow are common in many applications, including chemical, petroleum, pharmaceutical and food industries. Liquid-liquid phases are often contacted in stirred vessels. Therefore, the geometry of the tank and the type of used impeller are of great importance for producing desired drop size distribution (DSD). The impellers can be classified as producing shear or flow. Radial disc turbines like Rushton turbine, commonly used for liquid-liquid systems produce strong radial flow as well as intense turbulence. They can produce high interfacial area. Hydrofoil impellers like Lightnin A310 or Chemineer HE3 produce axial or mixed flow and are especially good for systems differing much in density of continuous and dispersed phase. They have blades mounted at a shallow angle to reduce drag at the leading edges, and provide intensive axial flow with small power requirements. They are able to achieve a just suspended state at a lower rotational speed than can disc turbines. Therefore, they are particularly suitable for solid-liquid systems [1,2]. However, it was shown that the low power number high flow agitators, like HE3 can be used for liquid-liquid dispersions and produce smaller droplets than high power number, high shear agitators at the same mean energy dissipation rates [3]. Therefore, in this paper the influence of impeller type on drop size distribution is presented. Two types of impellers are considered: 6-blade Rushton turbine (RT) and 3-blade high efficiency impeller (HE3). The distribution of locally averaged properties of turbulence including energy dissipation rate, ϵ , and scale of large eddies, L , are determined using CFD methods. The distribution of these properties in the stirred tank influences drop breakage and coalescence rates.

Both breakage and coalescence of droplets are taken into account. Breakage takes place in practice only in the impeller zone where energy dissipation rate is the highest. The zone in the stirred tank where coalescence is privileged depends on the drop deformation in the contact area and mobility of drop interfaces. Rates of both breakage and coalescence depend on the mean energy dissipation rate. Additionally, strong local variability of energy dissipation rate related to the internal intermittency (also called fine-scale intermittency) is taken into account. Fine-scale intermittency is described using multifractal formalism.

2. FORMULATION OF BREAKAGE AND COALESCENCE MODELS

The time evolution of drop size distribution in stirred tank is predicted by solving the population balance equation. Population of droplets of volume v and diameter d ($v = \pi d^3/6$) from inertial subrange of turbulence is considered. Population balance equation (in volume domain) for chemically equilibrated liquid-liquid dispersion (with no mass transport) and batch operation is given by

$$\begin{aligned} \frac{\partial n(v,t)}{\partial t} = & \frac{1}{2} \int_0^v h(v-v',v') \lambda(v-v',v') n(v-v',t) n(v',t) dv' - g(v) n(v,t) \\ & + \int_v^\infty \beta(v,v') v(v') g(v') n(v',t) dv' - n(v,t) \int_0^\infty h(v,v') \lambda(v,v') n(v',t) dv' \end{aligned} \quad (1)$$

In this equation $n(v,t)$ is number density of drops of volume v at time t (m^{-6}). Drop breakage rate $g(d) = g(v)$ (s^{-1}) in intermittent turbulent flow was developed by summing up the contributions to the break-up frequency from all vigorous eddies [4]

$$g(d) = C_g \sqrt{\ln(L/d)} \langle \varepsilon \rangle^{1/3} d^{-2/3} \int_{\alpha_{\min}}^{\alpha_x} (d/L)^{(\alpha+2-3f(\alpha))/3} d\alpha \quad (2)$$

C_g is constant ($C_g = 0.0035$), L is scale of large energetic eddies, α - multifractal exponent, and function $f(\alpha)$ denotes multifractal spectrum. Eddies that are vigorous enough to cause breakage are labelled by multifractal (scaling) exponent α from the range $\alpha_{\min} = 0.12$ (most vigorous eddies) to α_x (weakest eddies that can disperse the drop). The multifractal exponent α_x results from the balance between turbulent disruptive stresses and stabilizing stresses. When the dispersed phase viscosity is low the only stabilizing stress is generated due to interfacial tension and multifractal exponent α_x is given by [4]

$$\alpha_x = 2.5 \ln \left(L \langle \varepsilon \rangle^{0.4} \rho_C^{0.6} C_x^{-1} \sigma^{-0.6} \right) / \ln(L/d) - 1.5 \quad (3)$$

where C_x is a proportionality constant ($C_x = 0.23$). High dispersed phase viscosity μ_D increases the stabilising effect. The viscous stress inside the drop is generated when the drop deforms. In this case the upper limit of multifractal exponent, α_x , depends also on the dispersed phase viscosity. Furthermore, the new constant β_μ ($\beta_\mu = 1.91$) appears in the expression for α_x (for further details see [4]). Binary breakage (number of daughter drops $v(v') = 2$), and U-shaped daughter distribution function, $\beta(v,v')$ (m^{-3}), based on energetic considerations [5] are assumed.

Coalescence rate depends on drop collision frequency and coalescence efficiency. The average collision rate in intermittent turbulent field is calculated using the method of steepest descent [6]. Function $h(v, v') = h(d, d')$ ($m^3 s^{-1}$) appearing in population balance equation and characterising drop collision frequency is expressed as

$$h(d, d') = \sqrt{8\pi/3} \langle \varepsilon \rangle^{1/3} ((d + d')/2)^{7/3} ((d + d')/(2L))^{0.027} \quad (4)$$

The coalescence efficiency λ is determined by the ratio of average film drainage time $\langle t_c \rangle$ and average interaction time $\langle t_i \rangle$

$$\lambda = \exp(-C \langle t_c \rangle / \langle t_i \rangle) \quad (5)$$

where C is non-dimensional coefficient. Film drainage time, $\langle t_c \rangle$, depends on the mobility of drop interfaces. For pure liquid-liquid systems and low dispersed phase viscosity drop interfaces remain partially mobile, and film drainage is controlled by the flow inside the drop. Average drainage time in intermittent turbulent flow for deformed droplets with partially mobile interfaces can be expressed as follows [6]

$$\langle t_c \rangle \cong 0.25 \mu_D \tilde{a} R_{eq}^{3/2} \sigma^{-1} R_L^{-1/2} \left[(d_{jk}/L)^{0.016} / h_c - (d_{jk}/L)^{-0.01} / \tilde{h}_0 \right] \quad (6)$$

Expressions for film radius \tilde{a} , initial film thickness \tilde{h}_0 and critical film thickness h_c can be found elsewhere [6,7]. R_L is a radius of the larger droplet. Equivalent radius for unequal drops is defined as $R_{eq} = dd'/(d + d')$ and $d_{jk} = (d + d')/2$. Interaction time $\langle t_i \rangle$ is usually smaller than, or of the order of the time scale for two droplets to pass one another $\langle t_{ext} \rangle$. For intermittent turbulent flow the average time scale $\langle t_{ext} \rangle$ is then given by

$$\langle t_{ext} \rangle = \langle \varepsilon \rangle^{-1/3} ((d + d')/2)^{2/3} (2L/(d + d'))^{0.052} \quad (7)$$

However, for droplets of low viscosity the interaction time can be estimated as time resulting from droplet bouncing [6]

$$\langle t_i \rangle \cong 0.5 \left[8(\rho_D/\rho_C + 0.75) \rho_C R_s^3 / (3(1 + \xi^3) \sigma) \right]^{1/2} \quad (8)$$

where R_s is radius of smaller droplet, and $\xi = R_s / R_L$.

When the dispersed phase viscosity is high the drop interfaces are immobilized. In previous papers different cases were considered: undeformed droplets, deformed droplets with film radius resulting from the balance between the pressure caused by external force and the Laplace pressure, and deformed droplets with film radius proportional to the radius of smaller droplet [7,8]. It was shown that drops of high viscosity differing much in size, behave in a completely different way than other ones. In this paper the behaviour of large deformed droplets is considered. In this case the contact time, $\langle t_i \rangle = \langle t_{ext} \rangle$, is given by Eq. (7) and film drainage time is expressed as follows [8]

$$\langle t_c \rangle = 3 \mu_C \rho_C R_{eq}^4 \langle \varepsilon \rangle^{2/3} d_{jk}^{2/3} (d_{jk}/L)^{0.026} / (16 \sigma^2 h_c^2) \quad (9)$$

3. CFD MODEL

Turbulence properties for tanks equipped with one of the impellers: 6-blade Rushton turbine (RT) or three blade high efficiency impeller (HE3) are determined using CFD. Simulations are performed for tank of diameter $T = 0.15$ m, completely filled and closed. The aspect ratio is $H/T = 1$. The stirred tank is flat bottomed and fully baffled (four equally spaced baffles of width equal to $T/10$). It was assumed that impeller diameter to tank diameter ratio $D/T = 0.4$ and impeller clearance $C/T = 1/4$ for HE3. The high efficiency impeller has uniform blade width equal to 0.01 m. The blade angle is 30 degrees at the hub. The tip chord angle is 15 degrees. The blade is bent at 50% of its length. The thickness of blade is equal to 0.002 m. Rushton turbine has a diameter $D = 0.5 T$. A disc diameter is equal to $0.75D$, a blade thickness and disc thickness are $0.01D$.

The unstructured tetrahedral meshes with approximately $400\,000$ cells for Rushton turbine and $600\,000$ cells for high efficiency impeller were generated using Mixsim 2.1 software. 3D simulations were performed using finite volume package Fluent 6.3.26. The Multiple Reference Frame approach and standard $k-\varepsilon$ turbulence model with standard wall functions were used.

4. RESULTS AND DISCUSSION

CFD simulations were performed for high efficiency impeller (HE3) for impeller speed $N_{HE3} = 800$ rpm. Operating fluid was water. The presence of organic phase was not taken into account in these simulations. It was justified by low values of dispersed phase volume fraction ($\phi = 0.001$ for pure breakage and $\phi = 0.05$ for coalescence). For tank equipped with Rushton turbine simulations were performed for the impeller speed N_{RT} that was expected to give the same power input per unit mass ($N = 213$ rpm). These simulations allowed to determine power and flow numbers for both impellers: $P_o = 0.34$, $Fl = 0.39$ for high efficiency impeller, and $P_o = 4.98$, $Fl = 0.74$ for Rushton turbine. These values agree quite well with the measured ones ($P_o = 0.305$ and $Fl = 0.41$ for HE3 of $D/T = 0.46$ [9], $P_o = 0.3$ for HE3 of $D/T = 0.39$ and impeller clearance equal to $T/4$ [2]). Power number values for RT reported by different authors are in the range 4.6 to 6.3 . According to Bujalski et al. [10] correlation P_o depends on the tank size and impeller disc thickness. For $T = 0.15$ m and disc thickness equal to $0.01D$ the power number should be equal to 5.5 . However, their correlation was obtained for vessels of diameter from 0.22 m to 1.83 m. The flow generated by HE3 at clearance of $T/4$ has strong axial component directed to the base. Between the impeller hub and the tank base there is a weak reverse flow. Local values of the scale of large eddies were determined using calculated local values of energy dissipation rate, ε , and turbulent kinetic energy k , $L = (2k/3)^{3/2}/\varepsilon$. Contours of scales of large eddies for both types of impellers are presented in Figure 1. In both cases there is a distinct difference in large eddies size in the impeller zone and the bulk, though, average values of L in these zones do not differ as much as the values of energy dissipation rate do.

Earlier studies of the author have shown that the multiple cell model of tank (10-cells) predicts similar drop size distributions as 2-cell model provided that the impeller zone is properly defined [11]. For example, for Rushton turbine of $D/T = 1/3$ only part of impeller stream should be included into the impeller zone. However, in the case of RT of $D/T = 1/2$ that is considered here the whole discharge region is included to the impeller zone. This impeller stream region together with the impeller swept volume (extended here 3 mm above and 3 mm below impeller blades) occupies fraction $x_{imp} = 0.095$ of the tank volume. To determine mean values of energy dissipation rate and scale of large eddies auxiliary surfaces

were created and Surface Integrals function was used. Surfaces were separated by 1 mm in the impeller zone.

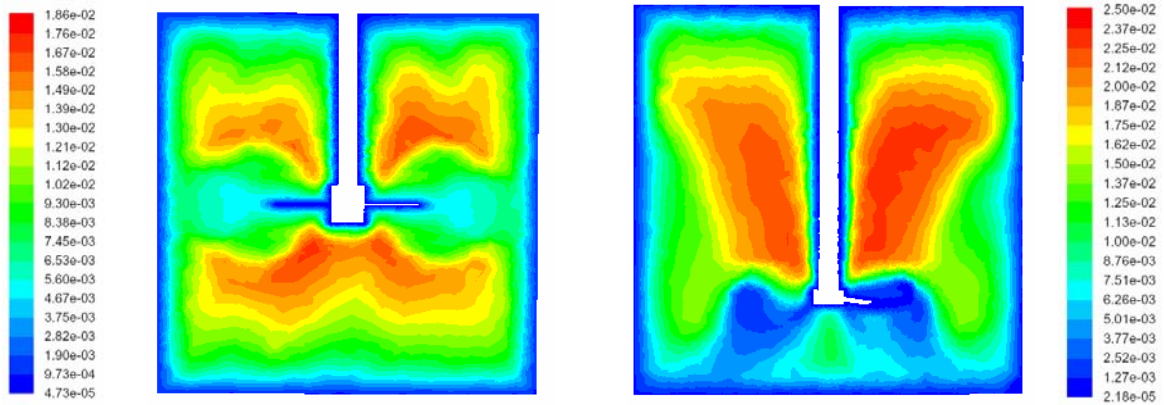


Fig. 1. Contours of large eddy scales for Rushton turbine and HE3 impeller (plane $\theta = 45^\circ$ between baffles).

Such densely created surfaces enable us to better define the limits of the impeller zone. For bulk zone surfaces were separated by 2 mm. The relative properties of turbulence for Rushton turbine of $D/T = 1/2$ are as follows: $\varphi_{\text{imp}} = \langle \varepsilon \rangle_{\text{imp}} / \langle \varepsilon \rangle = 6.1$, $\varphi_{\text{bulk}} = 0.465$, $L_{\text{imp}}/D = 0.0806$, $L_{\text{bulk}}/D = 0.13$. In the case of HE3 the impeller zone is defined as a cylinder of radius $r = 0.034$ m (slightly larger than impeller radius $R = 0.03$ m) and positioned between $z = 0.0325$ m and $z = 0.0425$ m. The volume fraction of this zone is equal to $x_{\text{imp}} = 0.0137$, normalized energy dissipation rate in this zone is $\varphi_{\text{imp}} = 45$, while in the bulk $\varphi_{\text{bulk}} = 0.389$. Normalized scales of large eddies are: $L_{\text{imp}}/D = 0.0573$ in the impeller zone and $L_{\text{bulk}}/D = 0.187$ in the bulk. The spatial distribution of energy dissipation rate in the impeller zone has been reported for RT by many researches. However, most of works were devoted to impellers of $D=T/3$. The percentage of the total energy dissipated in the impeller swept and impeller stream regions reported by different authors vary from 42 to 70 % [12]. Results for $D=T/2$ were presented by Okamoto et al. [13] and Zhou and Kresta [14]. According to Okamoto correlation $\varphi_{\text{imp}}=5.93$, $x_{\text{imp}}=0.105$, so the percentage of total energy dissipation in the impeller zone is 62.3%. Zhou and Kresta [14] measured 43.5% dissipation in the control volume containing impeller swept and impeller stream and occupying 0.1 of the tank volume. The percentage of total energy dissipation in the impeller region (57.95%) predicted in this work lies between these literature values.

Population balance equation was solved for two liquid-liquid systems. In the first case dispersed phase of low viscosity was considered ($\mu_D = 0.001$ Pa s). Density of the continuous phase was assumed to be $\rho_C = 1000$ kg/m³, and interfacial tension $\sigma = 0.035$ N/m. Second liquid-liquid system is characterized by $\mu_D = 0.5$ Pa s, $\rho_C = 1000$ kg/m³ and $\sigma = 0.0505$ N/m. For both liquid-liquid systems pure breakage (dispersed phase volume fraction $\phi = 0.001$) as well as breakage together with coalescence ($\phi = 0.05$) were simulated. In calculations constant C in Eq. (5) defining coalescence efficiency was assumed to be $C = 0.5$ for the first liquid-liquid system, and $C=0.1$ for the second. Hamaker constant that influences critical film thickness was assumed to be $A = 10^{-20}$ J (characteristic for pure liquid-liquid systems) and initial drop size $d = 3$ mm.

Figure 2 shows transient drop size distributions predicted for both types of impeller at equal power input per unit mass for conditions when only breakage takes place. Drop size distribution at short agitation time is much wider for HE3. However, mean Sauter diameter is

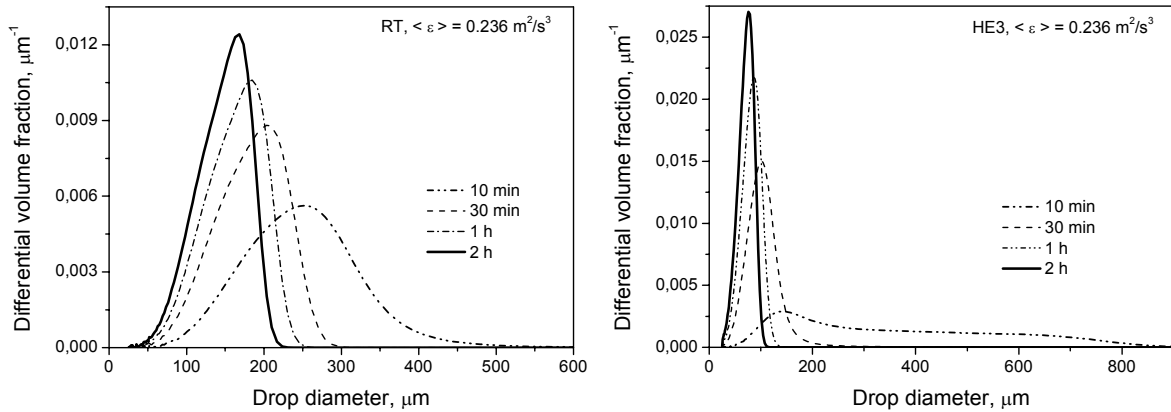


Fig. 2. Influence of impeller type on transient drop size distributions for dilute system ($\phi = 0.001$) with dispersed phase of low viscosity $\mu_D = 0.001$ Pas.

only slightly larger for HE3 than that for RT. This is because the largest volume fraction of drops is formulated by smaller droplets in the tank equipped with HE3 than in that equipped with RT. The higher $\langle \varepsilon \rangle$ the smaller d_{32} for HE3 in comparison with d_{32} for RT is observed even after a few minutes of agitation. But still the largest droplets are bigger for HE3 than for RT at short agitation time. After long agitation time droplets produced by HE3 are much smaller than droplets produced by RT. Comparison of DSDs and mean sizes of drops produced by different impellers after 2 h of agitation is shown in Fig 3. The described behaviour of droplets can be explained by smaller impeller zone volume and larger ϕ_{imp} in the tank equipped with high efficiency impeller. Very large droplets that are easily broken in both systems have greater chance to appear in the zone of high energy dissipation rate and, therefore, of high turbulent disruptive stresses, in the tank with RT ($x_{imp, RT} > x_{imp, HE3}$). However, final drop size is determined by the magnitude of ε_{imp} and this is much higher for HE3. Similar trends are observed for breakage of droplets of high viscosity, Fig. 4 and 5.

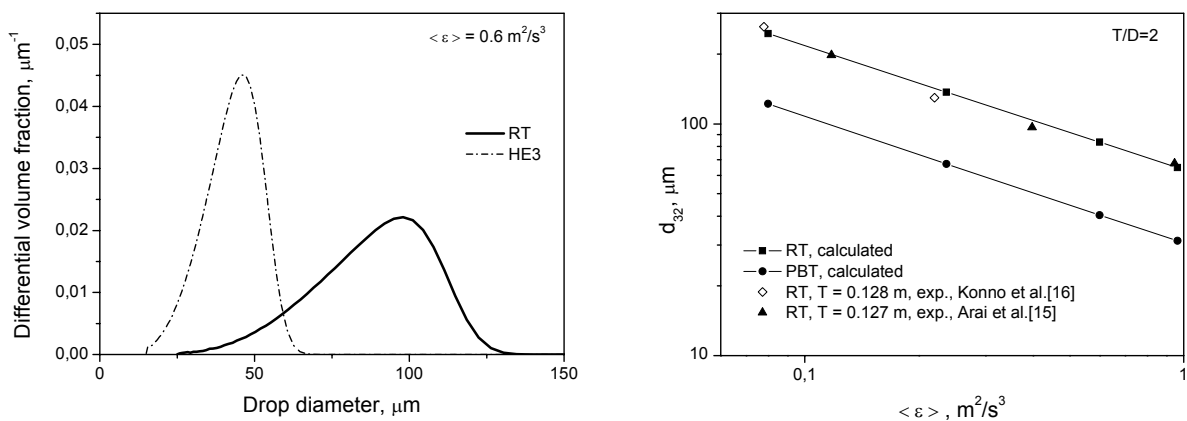


Fig. 3. Influence of impeller type on drop size distribution and Sauter diameter (pure breakage, $\mu_D=0.001$ Pas, $\phi=0.001$).

Breakage and coalescence models were previously verified experimentally for Rushton turbines of different D/T ratios. Comparison between measured (literature as well as own experiments) and predicted distributions (with energy dissipation rate distribution based on

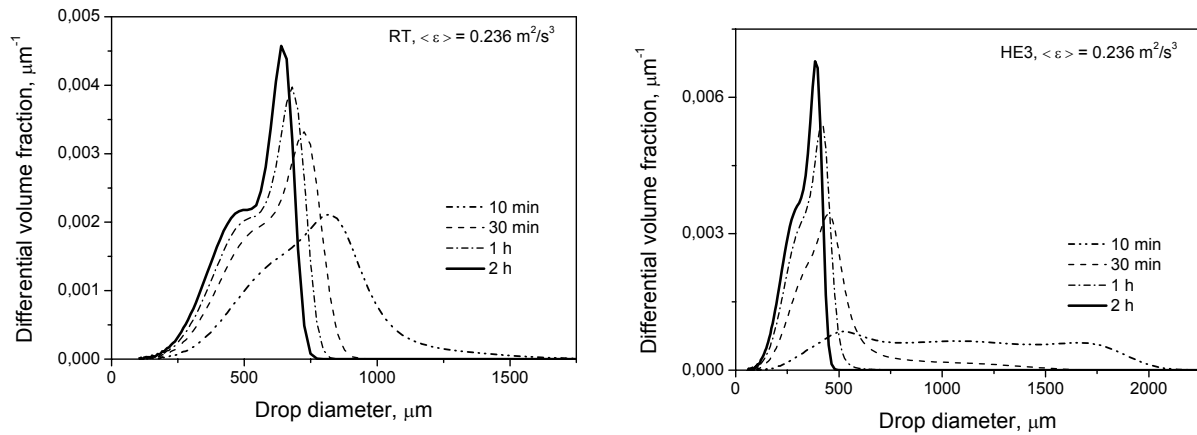


Fig. 4. Influence of impeller type on transient drop size distributions for dilute system ($\phi = 0.001$) with dispersed phase of high viscosity $\mu_D = 0.5$ Pas.

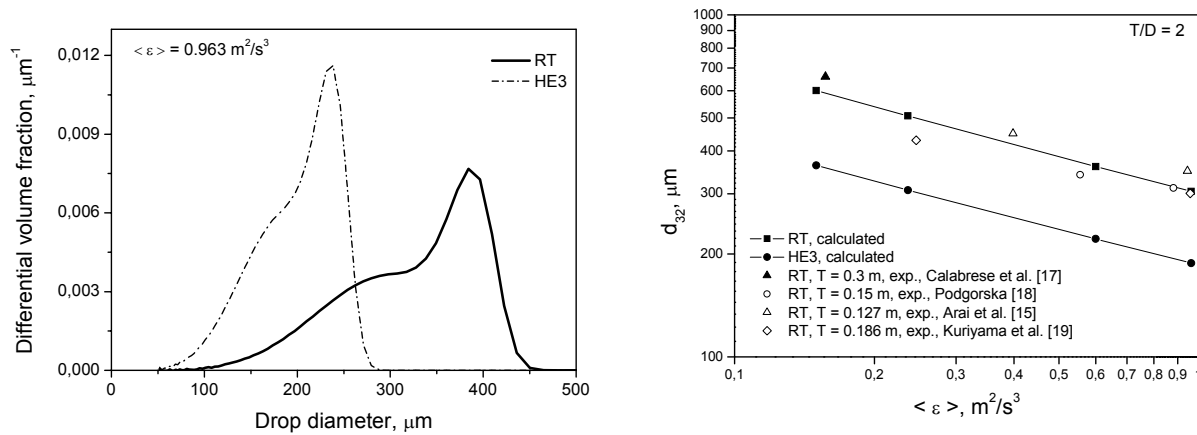


Fig. 5. Influence of impeller type on drop size distribution and Sauter diameter (pure breakage, $\mu_D=0.5$ Pas, $\phi=0.001$).

experimental Okamoto correlation as well as predicted using CFD) one can find elsewhere [4, 6-8, 11, 18]. Some literature experimental results (for long agitation time) for RT, $D=T/2$, for low as well as high dispersed phase viscosity are presented in Figures 3b and 5b. In the case of Arai et al. [15] experiments it was assumed that Sauter diameter $d_{32}=0.6d_{\max}$ (d_{\max} being the diameter of the largest stable drop) for dispersed phase of low viscosity and $d_{32}=0.5d_{\max}$ for dispersed phase of high viscosity. When the power number was not measured the $P_0=4.98$ was used to estimate power input per unit mass. Additional information is shown in Figures 3b and 5b. The agreement between model predictions and experimental data is quite good.

Figure 6a presents final drop size distributions (being the result of dynamic equilibrium between breakage and coalescence) produced by different impellers at higher dispersed phase volume fraction ($\phi = 0.05$) for pure liquid-liquid system (no surfactant) with dispersed phase of low viscosity. Under such conditions droplets have partially mobile interfaces and gentle collisions are preferred. Therefore, fast coalescence takes place in the bulk. The model predicts that at equal power input per unit mass droplets produced in both systems are similar. In the case of high dispersed phase viscosity coalescence is highly hindered by immobilization of drop interfaces. However, very wide drop size distributions are usually

observed for such dispersions and as was shown earlier, droplets differing in size or in deformation in the drop contact area behave in a completely different way [8]. Coalescence of small rigid drops or small slightly deformed drops may be even faster in the zone of high energy dissipation rate than in the bulk. However, the largest volume fraction of population (being the result of dynamical equilibrium between breakage and coalescence) is occupied by large deformed droplets. Their behaviour can be predicted using Eqs (7) and (9). Predicted drop size distributions are shown in Fig. 6b. Slightly smaller droplets are produced by HE3.

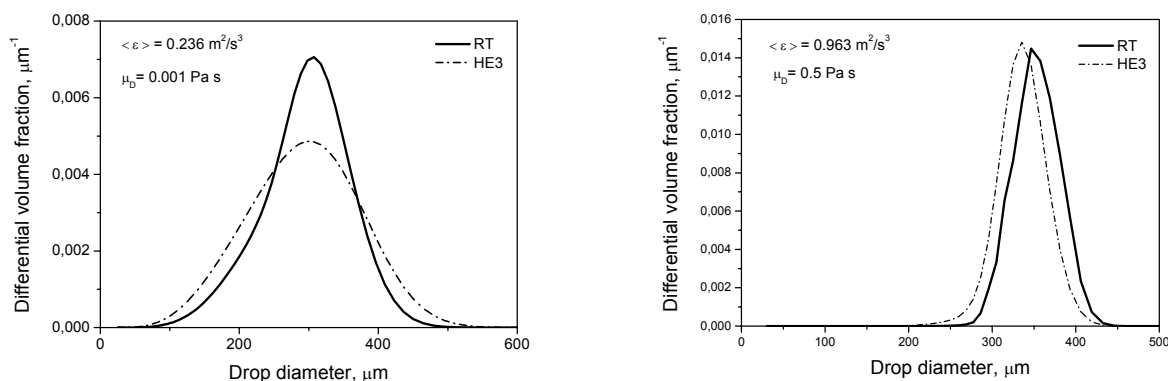


Fig. 6. Influence of impeller type on drop size distribution in fast coalescing dispersion ($\mu_D=0.001 \text{ Pa s}$, $\phi=0.05$) and slow coalescing dispersion ($\mu_D=0.5 \text{ Pa s}$, $\phi=0.05$).

ACKNOWLEDGEMENT

This work was financed from the Budget for Science by Polish Ministry of Science in 2008-2011.

3. REFERENCES

- Atiemo-Obeng V.A., Roy Penny W., Armenante P., 2004. "Solid-liquid mixing", in: *Handbook of Industrial Mixing. Science and Practice* (E.L. Paul, V.A. Atiemo-Obeng and S.M. Kresta, eds), Chapter 10, Wiley-Interscience, Hoboken, pp. 543-584.
- Ibrahim S., Nienow A.W., 1995, *Trans IChemE*, **73**, Part A, 485-491.
- Pacek A.W., Chamsart S., Nienow A.W., Bakker A., 1999, *Chem. Eng. Sci.*, **54**, 4211-4222.
- Bałdyga J., Podgórska W., 1998, *Can. J Chem. Eng.*, **76**, 456-470.
- Tsouris C., Tavlarides L.L., 1994, *AIChEJ*, **40**, 395-406.
- Podgórska W., Bałdyga J., 2001, *Chem. Eng. Sci.*, **56**, 741-746.
- Podgórska W., 2005, *Chem. Eng. Sci.*, **60**, 2115-2125.
- Podgórska W., 2007, *Trans IChemE, Part A, Chem. Eng. Res. Des.*, **85**(A5), 721-729.
- Jaworski Z., Nienow A.W., Dyster K.N., 1996, *Can. J. Chem. Eng.* **74**, 3-15.
- Bujalski W., Nienow A.W., Chatwin S., Cooke M., 1987, *Chem. Eng. Sci.*, **42**, 317-326.
- Podgórska W., Bałdyga J., 2002, *17th International Symposium on Chemical Reaction Engineering ISCRE 17*, Paper MS0398, Hong Kong, pp. 1-21.
- Ng K., Yianneskis M., 2000, *Trans IChemE, Part A*, **78**, 334-341.
- Okamoto Y., Nishikawa M., Hashimoto K., 1981, *Int. Chem. Eng.*, **21**, 88-94.
- Zhou G., Kresta S.M., 1996, *Trans IChemE, Part A*, **74**, 379-389.
- Arai K., Konno M., Matunaga Y., Saito S., 1977, *J. Chem. Eng. Japan*, **10**, 325-330.
- Konno M., Aoki M., Saito S., 1983, *J. Chem. Eng. Japan*, **16**, 312-319.
- Calabrese R.V., Chang T.P.K., Dang P.T., 1986, *AIChEJ*, **32**, 657-666.
- Podgórska W., 2006, *Chem. Eng. Sci.*, **61**, 2986-2993.
- Kuriyama M., Ono M., Tokanai H., Konno H., 1996, *Trans IChemE, Part A*, **74**, 431-437.